Day-night cold trap for Titanium oxide in hot-Jupiter atmosphere

Vivien Parmentier[1] and Adam P. Showman[2]

[1] Université de Nice-Sophia Antipolis, Observatoire de la Côte d'Azur, CNRS UMR 6202, Nice, France

[2] Department of Planetary Sciences and Lunar and Planetary Laboratory, The University of Arizona, Tucson, USA

July 2011, ISIMA, Beijing

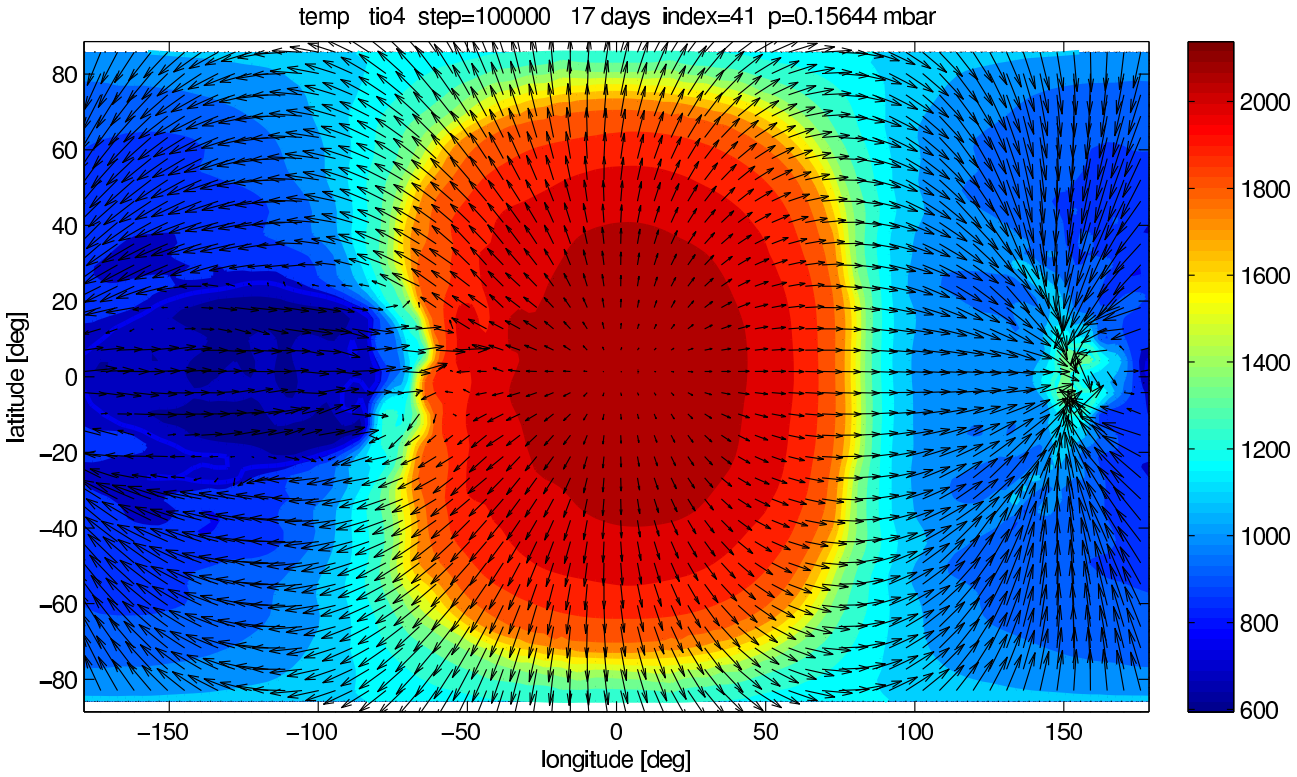

Abstract

Temperature inversion leading to a hot stratosphere have been observed in some hot-Jupiter. Theoretical models predict that such a temperature inversion can be caused by the presence of a strong absorber in the visible in the high atmosphere. Titanium oxide have been proposed to be a good candidate for being this extra-absorber. Although the temperature in the day side of these planets can be high enough to maintain titanium oxide in a gaseous phase, it is not the case in the night side. In this work we discuss how the day/night temperature contrast can lead to the depletion of titanium oxide in the high atmosphere of hot-Jupiter. Using 1D and 3D models we found some constraints on the vertical diffusion coefficient needed to maintain enough titanium oxide in the upper atmosphere to create a temperature inversion. These constraints are similar to the ones given by Spiegel et al. (2009) for the vertical cold trap but hold for all the planets, even the ones that are too hot to be affected by the vertical cold trap.

Contents

Introduction

Why do we care about Titanium oxide ?

A wide variety of hot-Jupiters have been discovered in the past few years. Most of them orbit so close to their star that they are tidally locked : they have a day-side always facing the star and a night side always facing the opposite direction. Day-side and night side temperature have been measured for some of these planets. Values from 2200K at the limb of HD209458b (Lecavelier Des Etangs et al. (2008)) to 3120K in the day-side in Wasp-18b by Nymeyer et al. (2011) have already been measured. At these very high temperatures, components that are usually condensed in planetary atmosphere can become thermodynamically stable in the gas phase over some parts of the planet. It is the case for titanium oxide (hereafter TiO) : with a condensation temperature around 1900K it can remain in the atmosphere of these planets. Actually TiO is a well known coumpound of brown dwarfs ; the presence or absence of its absorption bands sets the boundary between M dwarf and L dwarf stars(Lodders (2002)).

High signal to noise ratio spectra of the day-side of some hot-Jupiter atmospheres have been measured using the Spitzer space telescope (Charbonneau et al. (2008), Knutson et al. (2008), Deming et al. (2011), Machalek et al. (2009), Machalek et al. (2010), Todorov et al. (2010), Fressin et al. (2009)). The spectra have a low spectral resolution, due to the small number of observation channels of the IRAC instrument on the Spitzer space telescope. However, some of these spectra show a flux excess at $4.5\mu m$, which has been interpreted as emission rather than absorption bands due to a temperature inversion in the atmosphere. This kind of temperature inversion is expected by theoretical models when a strong absorber in the visible is present in the upper atmosphere (Hubeny et al. (2003), Fortney et al. (2006), Fortney et al. (2008). Though there is no unambiguous direct detection of titanium oxide bands (Désert et al. (2008)), it seems a good candidate for being this absorber.

Vertical cold trap

The atmospheres of hot-Jupiter are heterogeneous and dynamically active. Therefore in some parts of the planet, gaseous TiO might be stable whereas in some other parts it should condense out.

Vertically, the atmosphere is not at all isothermal. In presence of a temperature inversion, the hot stratosphere is above colder layers where the titanium oxide might condense and be trapped, depleting the stratosphere. This vertical cold trap has been studied by Spiegel et al. (2009). They obtain constraints on the vertical diffusion coefficient necessary to have enough TiO in the high atmosphere to create a temperature inversion.

Horizontal cold trap

Several teams have been using the Spitzer space telescope in order to monitor the full orbit of a hot-Jupiter in the infrared. This type of observations can lead to two very useful measurements : the day/night temperature contrast of the planet and the displacement of the hottest point of the planet east or west of the substellar point. The measured day/night temperature contrast ranges from ∼240K for HD189733b (Knutson et al. (2008)) to more than 900K for υ Andromeda b. (Crossfield et al. (2010)). The efficiency of the energy redistribution between the day-side and the night-side depends on the dynamics of the atmosphere. Showman & Guillot (2002) predicted the formation of an eastward jet advecting the energy from the day side to the night side. Measurement of the eastward displacement of the hottest point of the planet confirmed the existence of this jet and enabled its speed to be measured (∼1 km/s). This eastward jet appears in most of global circulation models (Showman & Polvani (2011), Showman et al.

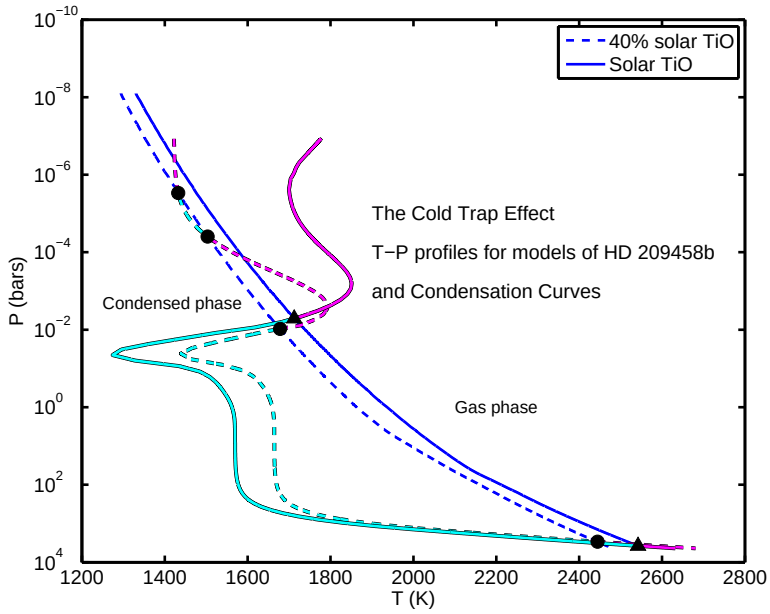

Figure 1: Illustration of the cold-trap phenomena from Spiegel et al. (2009). The blue curve is the condensation curve for TiO. The other one is the temperature profile for HD209458b. The temperature profiles crosses the condensation line for TiO at different heights, leading to a possible depletion of TiO in the stratosphere.

(2008)) and is known to be a main feature of hot-Jupiter atmospheric dynamic. When TiO is advected from the day side to the night side, it should condense and rain out leading to a stratospheric depletion. This is what we call the horizontal cold trap. Depending on the strength of the jet and the efficiency of the diffusion, TiO particles might or might not survive in the upper atmospheres of hot-Jupiter.

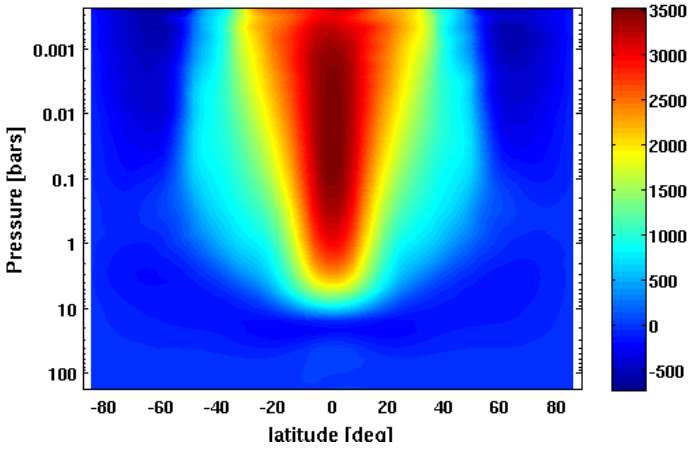

Figure 2: Zonal mean speed in HD189733b from Showman et al. (2009). The speeds are given in $ms^{-1}$and are eastward. We can see that the equatorial jet extend from 1bar to less than 1mbar.

1 Settling velocity of a particle in the atmosphere

1.1 Stokes flow

The problem of a flow past a sphere in a laminar and continuous flow have been solved by Stokes in 1851. The solution is described in Pruppacher & Klett (1978) and leads to a drag force given by :

$$F_{Drag} = 6Ua\eta \tag{1}$$

where a is the radius of the particle, η is the dynamic viscosity of the fluid and U the relative velocity between the fluid and the particle. We define the drag coefficient, C_D by :

$$C_D = \frac{F_{drag}}{\rho U_\infty^2 \pi a^2/2} \tag{2}$$

Using Stokes solution for the drag gives :

$$C_{D_{Stokes}} = \frac{24}{N_{R_e}} \tag{3}$$

where the Reynolds number is given by :

$$N_{R_e} = 2R_e = \frac{2\rho U a}{\eta} \tag{4}$$

with ρ the density of the fluid.

Equating gravity and drag forces leads to the settling velocity of a particle in an atmosphere:

$$\frac{4}{3}\pi a^3(\rho_p - \rho) = \frac{\rho V_f^2 \pi a^2}{2} C_D \tag{5}$$

with ρ_p the density of the particle. That leads to :

$$V_f^2 C_D = \frac{8a}{3}\frac{\rho_p - \rho}{\rho} \tag{6}$$

For Stokes flow we replace C_D by its expression from equation 3 and get :

$$V_f = V_{stokes} = \frac{2a^2 g(\rho_p - \rho)}{9\eta} \tag{7}$$

We are using the viscosity of hydrogen given by Rosner (2000)

$$\eta = \frac{5}{16}\frac{\sqrt{\pi m k_B T}}{\pi d^2}\frac{(k_B T/\epsilon)^{0.16}}{1.22} \tag{8}$$

where d is the molecular diameter and ϵ is the depth of the Lennard-Jones potential well for the atmosphere (2.827×10^{-8} cm and $59.7 k_B$ K for H_2). The validity of this expression is in agreement with the experimental values from Stiel & Thodos (1963).

1.2 Cunningham velocity

When the density of the flow becomes so small that the mean free path of the particles becomes of the order of the size of the particles, the continuity approximation used in the Stokes formalism is no longer valid around the object and kinetic effects have to be taken into account. In particular, the no-slip boundary condition is broken : the molecules at the surface of the object can't be considered at rest. These effects have been calculated by Cunningham (1910) leading to a smaller drag coefficient of the form :

$$C_D = \frac{C_{DStokes}}{\beta} \tag{9}$$

where β is the Cunnhingham factor. This factor have been first determined by Cunningham as $\beta = 1 + 1.63\frac{\lambda}{a}$ and refined later many authors. We decided to use the value from Li & Wang (2003) which is the same choice as Spiegel et al. (2009).

$$\beta = 1 + K_N(1.256 + 0.4e^{-1.1/K_N}) \tag{10}$$

where the Knudsen number is the ratio of the mean free path to the size of the particle :

$$K_N = \frac{\lambda}{a} \tag{11}$$

and the mean free path can be expressed as :

$$\lambda = \frac{1}{\sqrt{2}\pi n d^2} \tag{12}$$

where d is the size of the molecules and n their density. For a perfect gas we obtain :

$$\lambda = \frac{k_B T}{\sqrt{2}\pi d^2} \frac{1}{P} \tag{13}$$

where P is the gas pressure.

The Cunningham drag from equation 9 leads to a settling velocity of :

$$V_f = V_{Cunningham} = \beta V_{Stokes} \tag{14}$$

In the high pressure regime, the Knudsen number goes to zero and the cunningham velocity becomes equal to the Stokes velocity. In the low pressure regime, the Knudsen number becomes very big and we get :

$$V_{Cunningham} \sim 1.656 K_N V_{Stokes} \tag{15}$$

Using equations 11 and 13 we get :

$$V_{Cunningham} \propto \frac{1}{P} \tag{16}$$

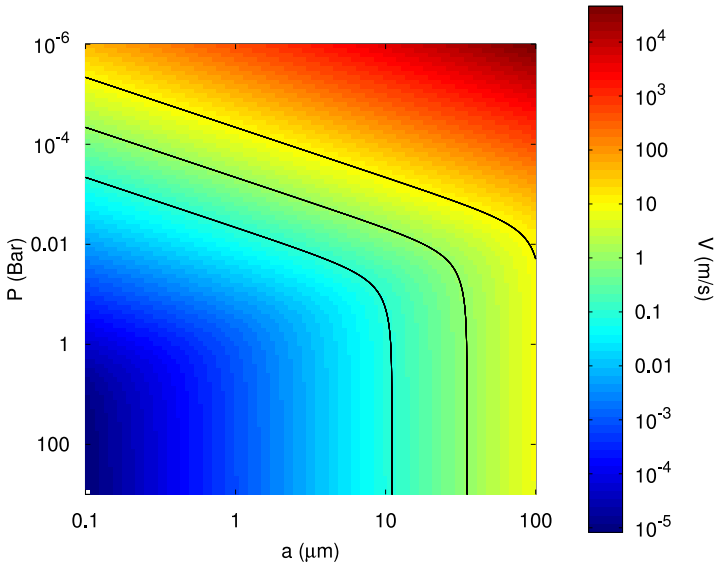

Figure 3: Cunningham velocity in function of pressure and particle size. From bottom to top the black lines correspond to 0.1 m.s^{-1}, 1 m.s^{-1}and 10 m.s^{-1}. We can see the stokes regime, where the velocity is independent of the pressure and the Cunningham regime where the velocity is inversely proportional to the pressure.

1.3 Correction to the Cunningham velocity

As shown in figure 3, the Cunningham velocity can reach very high values for big particles in the low pressure regime. We refined the model for big Reynolds number using the equations of Probstein (1968). The velocity correction being less than one order of magnitude, we decided to use the Cunningham velocity in the model. The derivation of the deviations from the Cunningham velocity is described in appendix

2 Application to falling particles in an atmosphere : 1D model

In order to have a better understanding of the problem we built a 1D model of the equilibrium between downward settling and upward turbulent mixing of particles in an atmosphere. Our system is a vertical column atmosphere which is advected around the planet. On the day side we consider that the TiO particles are gaseous and only vertical turbulent mixing processes are relevant. On the night side we consider that TiO condense into particle of size a, so both turbulent mixing and settlement are relevant.

2.1 Equations

The equation for the concentration of the particles is derived from the conservation equation :

$$\frac{D\chi}{Dt} = \frac{1}{\rho}\frac{\partial(\rho\chi V_f)}{\partial z} \tag{17}$$

where χ is the mass of particles per unit mass of gas in which they are suspended and wV_f the settling velocity of the particles. This equation is a three dimensional equation for the particle density. We will now assume that averaging over latitude and longitude, this equation becomes a vertical diffusion equation. This is a big assumption : it is not obvious that the average particle concentration should follow a diffusion equation and we should keep this caveat in mind when interpreting the results of this model. However, Holton (1986) showed that this assumption can be true when parametrizing the meridional flow. Then the 1D equation becomes

$$\frac{\partial\chi}{\partial t} - \frac{1}{\rho}\frac{\partial}{\partial z}\left(\rho K_z \frac{\partial\chi}{\partial z}\right) = \frac{1}{\rho}\frac{\partial(\rho\chi V_f)}{\partial z} \tag{18}$$

where K_z is the vertical diffusion coefficient. Using hydrostatic balance, we transform to P as the vertical coordinate :

$$\frac{\partial\chi}{\partial t} - \frac{\partial}{\partial P}\left(\rho^2 K_z \frac{\partial\chi}{\partial P}\right) = -\frac{1}{g}\frac{\partial(\rho\chi V_f)}{\partial P} \tag{19}$$

Using the perfect gas law for the atmosphere we get :

$$\frac{\partial\chi}{\partial t} - \frac{\partial}{\partial P}\left(P^2\left(\frac{mg}{k_B T}\right)^2 K_z \frac{\partial\chi}{\partial P}\right) = -\frac{\partial(\frac{mg}{k_B T}P\chi V_f)}{\partial P} \tag{20}$$

We can define the diffusive time scale as $\tau_d = \frac{H^2}{K_z}$ and a reference free fall time scale using the stokes velocity $\tau_S = H/V_{Stokes}$ with $H = \frac{k_B T}{mg}$ the atmospheric scale height and V_{Stokes} the stokes velocity defined in equation 7. We note that τ_S is a reference time scale and will not be equal to the effective free fall time scale for big Knudsen number. The equation becomes :

$$\frac{\partial\chi}{\partial t} - \frac{\partial}{\partial P}\left(\frac{P^2}{\tau_d}\frac{\partial\chi}{\partial P}\right) = -\frac{1}{\tau_S}\frac{\partial\beta P\chi}{\partial P} \tag{21}$$

2.2 Steady-state solutions

Although in reality air parcels will travel from day to night and will thus alternately experience conditions with and without particle settling (on the night and day side respectively) it is useful

to consider a simple analytic steady-state solution for the case where diffusion and settling are both always present. Then the steady state solutions of equation 21 are solutions of :

$$P^2 \frac{\partial \chi}{\partial P} - \beta \frac{\tau_d}{\tau_S} P \chi = C \tag{22}$$

where C is a constant. When P goes to 0, χ goes to 0 and we assume that $\frac{\partial \chi}{\partial P}$ does not go to infinity. Then the constant must be zero and we obtain :

$$\frac{\partial \chi}{\partial P} = \frac{\beta}{P} \frac{\tau_d}{\tau_S} \chi \tag{23}$$

In order to simplify the problem, we will forget about the transitional regime for β from equation 10 and use the expression :

$$\beta = 1 + 1.656 K_N \tag{24}$$

Then, considering K_z constant we obtain the following solution :

$$\chi_{eq} = \chi_0 \left(\frac{P}{P_0} \right)^{\frac{\tau_d}{\tau_S}} e^{-\frac{\tau_d}{\tau_S} \frac{1.617 k_B T}{\sqrt{2} \pi a d^2} \left(\frac{1}{P} - \frac{1}{P_0} \right)} \tag{25}$$

As it can be seen in the figure 5, the equilibrium profile is either constant or decreases very strongly with height. We thus follow the criterion given by Spiegel et al. (2009) : there should be an abundance of TiO at 1mbar greater than 0.5 the deep interior abundance to create a temperature inversion. For a given size of particle, a given diffusion coefficient is needed to maintain this abundance. We plotted the values of the diffusion coefficient in figure 4. The results we obtain are very similar to those of Spiegel et al. (2009) for the vertical cold trap but are independent of the gravity and thus the planet considered.

In equation 25 we can see two different regimes : for small particle radius, the exponential decrease will be dominant whereas for big particles the factor inside the exponential decreases and the dominant term will be the power law. Thus to reach our criterion $\chi_{lim} = \frac{\chi}{\chi_0} = 0.5$ at $P_{lim} = 1$ mbar for the small particles case we neglect the value of the power law term and get :

$$\frac{\tau_d}{\tau_S} \frac{1.617 k_B T}{\sqrt{2} \pi a d^2} \left(\frac{1}{P} - \frac{1}{P_0} \right) = -\ln(\chi_{lim}) \tag{26}$$

Choosing $P_0 >> P_{lim}$, replacing τ_d and τ_S by their expression and using equation 8 for the mean free path we obtain a condition on the diffusion coefficient :

$$K_{z_{lim}} \sim -1.656 \frac{0.613}{\sqrt{\pi} \ln(\chi_{lim})} \left(\frac{k_B T}{\epsilon} \right)^{-0.16} \left(\frac{k_B T}{m} \right)^{3/2} \rho_p \frac{a}{P_{lim}} \tag{27}$$

For the big particles we neglect the exponential term and the condition needed is :

$$\frac{\tau_d}{\tau_S} \sim \frac{\ln(\chi_{lim})}{\ln(P_{lim}) - \ln(P_0)} \tag{28}$$

that leads to :

$$K_{z_{lim}} \sim \frac{2}{9} \frac{k_B T}{m} \frac{\rho_p}{\eta} \frac{\ln(P_{lim}/P_0)}{\ln \chi_{lim}} a^2 \tag{29}$$

Again we note that these limits for the diffusion coefficient are independent of the planet considered.

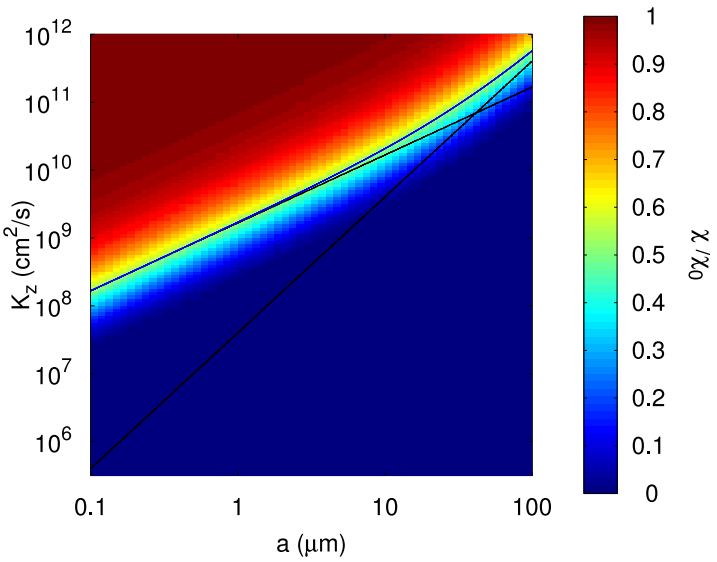

Figure 4: Equilibrium abundance of TiO at 1mbar as a function of the size of the particle and the vertical diffusion coefficient. To form a temperature inversion requires the abundance to be at least 0.5 at 1mbar. The black lines are the diffusion coefficient calculated by equations 27 and 29. The blue line is the sum of these two coefficient.

2.3 Departure from equilibrium

The very fast atmospheric circulation in hot-Jupiter might lead to non-equilibrium solutions for the particle density in the atmosphere. We consider numerical solutions for the case where moving air parcels experience alternately nightside condition (where TiO condenses and settles) and dayside conditions (where it sublimates to gas phase and hence does not settle) We solved equation 21 for a column of air which is forced to a day/night alternation of 24 hours. This correspond to a column of air advected by an eastward jet of 3.3 km/saround HD209458b. While on the night side, particles are diffused vertically but are also falling at the Cunningham velocity whereas in the day side they are only diffusing. Figure 5 shows the vertical profiles of TiO for a 10 µm condensate at each hour throughout one day-night cycle once the numerical solution has reached a periodic equilibrium. We see that the profiles are not exactly at equilibrium value and that there is a small day-night contrast. To visualize better this departure from equilibrium, figure 6 shows the needed diffusion coefficient to achieve 0.5 abundance of TiO at 1mbar for the profile at equilibrium (corresponding to the isocontour of figure 4), for the profile at the day/night terminator and for the profile at the night/day terminator. Small particles fall slowly, for that reason the curve for small particles doesn't vary during the day or the night but never reaches the equilibrium value. Big particles settle more rapidly so the curve for big particles reaches its equilibrium value during the night and the day/night amplitude is quite big.

3 Application to falling particles in an atmosphere : 3D model

In order to get more realistic constraints on the TiO abundance in hot-Jupiters, we decided to use the full 3D global circulation model described in Showman et al. (2009). In a first step, we concentrate on the case of HD209458b as a proxy for other hot-Jupiters. Even if for the specific case of HD209458b, the vertical cold trap might be of greater importance than the horizontal one, the lack of stable model for hotter planet motivated our decision to use this planet as an example. We turned on a package modeling passive tracers in the atmosphere of the planet and modified its source term in order to take into account the settling of the particles. We assume that the diffusion due to the flow is greater than the molecular diffusion and that the resolution is good enough to capture the main feature of the tracer diffusion. For that reason we didn't add any diffusive term in the tracer equation. We artificially define the day/night

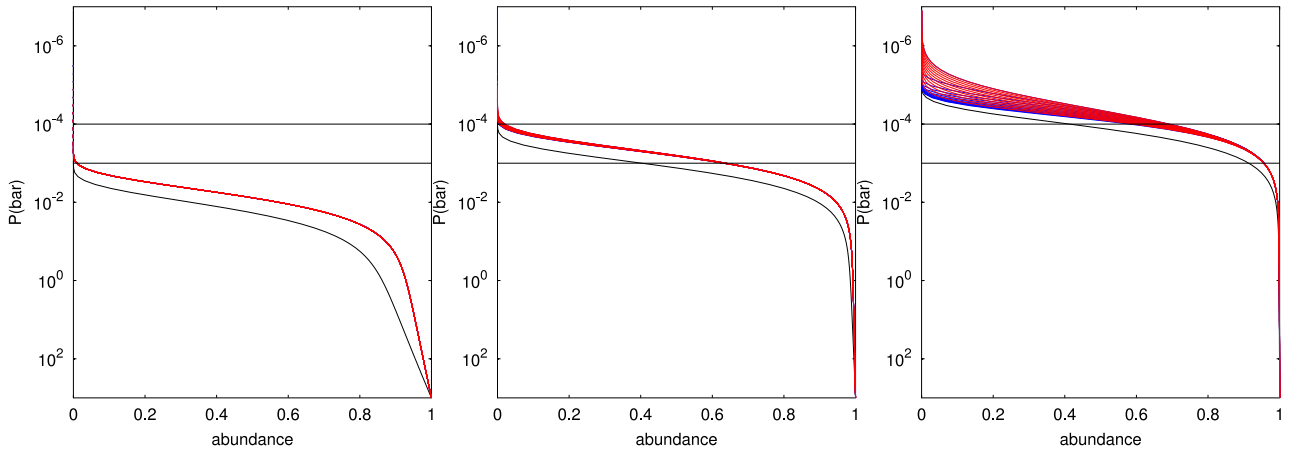

(a) $K_z = 10^8 cm^2/s$ (b) $K_z = 10^9 cm^2/s$ (c) $K_z = 10^{10} cm^2/s$

Figure 5: Abundance profiles for each hour thought a day-night cycle. The curves in blue are the night side profiles while the curves in red are the day-side profiles. The black line is the equilibrium profile. The two horizontal lines represent the 1 and 0.1mbar levels.

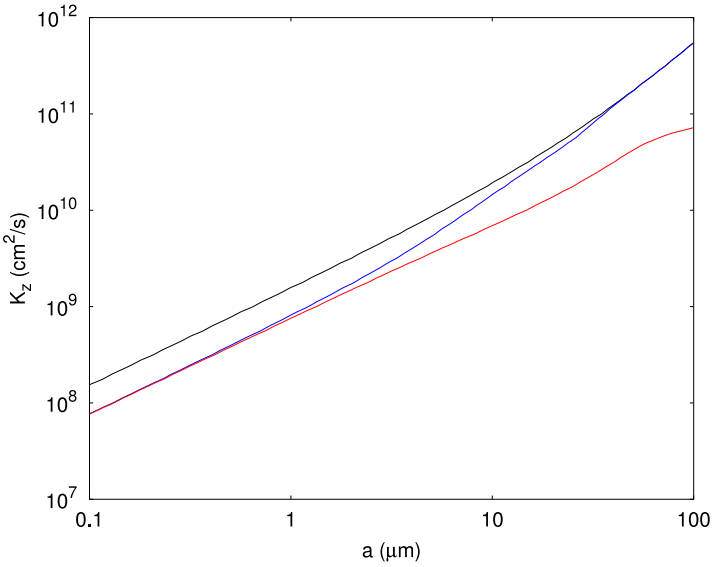

Figure 6: Diffusion coefficient needed to maintain an abundance of 0.5 at the 1mbar level. the equilibrium case is in blue, the day/night terminator in red and the night/day terminator in blue.

boundary as being the limit between gaseous and condensed particles. The model only run for 21 day for the moment and some improvement have yet to be done but the first results are presented in figure 7 and 8. In figure 8 for a 1 µm condensate, we can see clearly that the upper atmosphere is depleted in the night side but the particle transport seem sufficiently efficient to maintain a high abundance of TiO in the day side. What can be seen in the two figure is that the vertical transport of the tracer seems more sophisticated than a simple diffusion, what should be understood in order to compare the results from the 1D model with the results from the 3D model.

Conclusion

We developed a one-dimensional model for falling particles in an atmosphere. We show that the day/night cold trap in hot-Jupiters can be as important as the vertical one for the depletion of TiO. We give constraints on the diffusion coefficient needed to maintain enough TiO in the upper atmosphere to create a temperature inversion. These constraints are similar to the ones given by Spiegel et al. (2009) for the vertical cold trap but hold for all the planets, even the

ones that are too hot to be affected by the vertical cold trap. Now we need to continue the 3D simulations in order to have a better understanding of the influence of the dynamic on the TiO abundance in the atmosphere.

Acknowledgment

I would like to thank Adam Showman for being present during the six weeks of ISIMA, he was a very good advisor and also a good swimming companion. Thanks to Andrew Cumming for useful discussion. I thank Pascale Garaud and all the people who made this program possible. Finally thanks to all the students and professors who were in Beijing for contributing to a very nice working (and not only working !) environment.

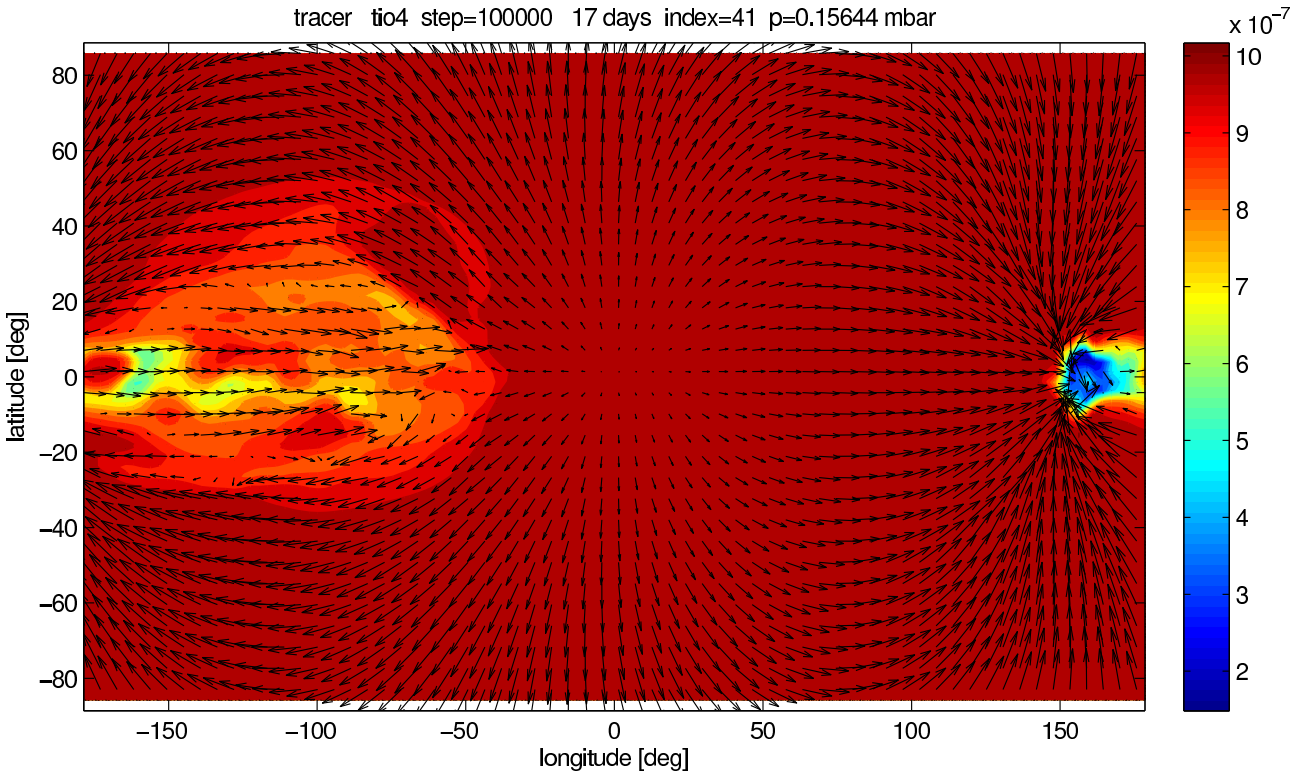

Figure 7: Horizontal slide at the 0.15 mbar level of TiO abundance after 21 days of integration for a condensate size of 1 µm. The arrows represents the wind speed and directions. You can already see the eastward jet forming.

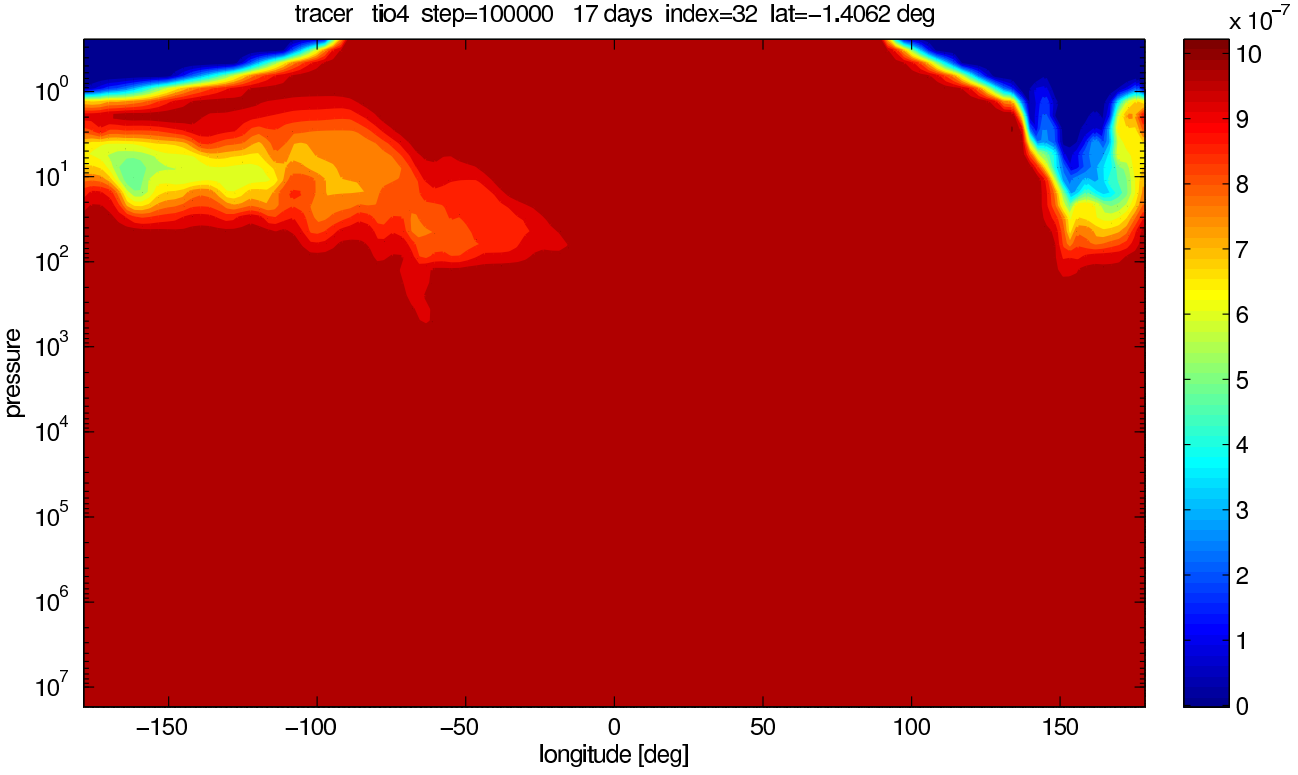

Figure 8: Vertical slice of the atmosphere of HD209458b along the equator. The condensate size is 1 µm. The abundance of TiO is represented by the colorscale.

References

Ackerman, A. S. & Marley, M. S. 2001, *ApJ*, 556, 872

Chapman, S. & Cowling, T. 1970, The mathematical theory of non-uniform gases, 3rd edn. (Cambridge mathematical library)

Charbonneau, D., Knutson, H. A., Barman, T., et al. 2008, *ApJ*, 686, 1341

Crossfield, I. J. M., Hansen, B. M. S., Harrington, J., et al. 2010, *ApJ*, 723, 1436

Cunningham, E. 1910, Proceedings of the Royal Society of London. Series A, Containing Papers of a Mathematical and Physical Character, 83, pp. 357

Deming, D., Knutson, H., Agol, E., et al. 2011, *ApJ*, 726, 95

Désert, J.-M., Vidal-Madjar, A., Lecavelier Des Etangs, A., et al. 2008, *Astron. & Astrophys*, 492, 585

Fortney, J. J., Lodders, K., Marley, M. S., & Freedman, R. S. 2008, *ApJ*, 678, 1419

Fortney, J. J., Saumon, D., Marley, M. S., Lodders, K., & Freedman, R. S. 2006, *ApJ*, 642, 495

Fressin, F., Guillot, T., & Nesta, L. 2009, *Astron. & Astrophys*, 504, 605

Holton, J. R. 1986, Journal of Geophysical Research, 91, 2681

Hubeny, I., Burrows, A., & Sudarsky, D. 2003, *ApJ*, 594, 1011

Knutson, H. A., Charbonneau, D., Allen, L. E., Burrows, A., & Megeath, S. T. 2008, *ApJ*, 673, 526

Lecavelier Des Etangs, A., Vidal-Madjar, A., Désert, J.-M., & Sing, D. 2008, *Astron. & Astrophys*, 485, 865

Li, Z. & Wang, H. 2003, Physical Review E - Statistical, Nonlinear and Soft Matter Physics, 68, 061206

Lodders, K. 2002, *ApJ*, 577, 974

Machalek, P., Greene, T., McCullough, P. R., et al. 2010, *ApJ*, 711, 111

Machalek, P., McCullough, P. R., Burrows, A., et al. 2009, *ApJ*, 701, 514

Nymeyer, S., Harrington, J., Hardy, R. A., et al. 2011, ArXiv e-prints

Probstein, R. F. 1968, Problems of hydrodynamics and continuum mechanics (Society for industrial and applied mathematics)

Pruppacher, H. & Klett, J. 1978, Microphysics of clouds and precipitation (D. Reidel publishing compagny)

Rosner, D. E. 2000, Transport processes in chemically reacting flow systems (Dover : Mineola)

Showman, A. P., Fortney, J. J., Lian, Y., et al. 2009, *ApJ*, 699, 564

Showman, A. P. & Guillot, T. 2002, *Astron. & Astrophys*, 385, 166

Showman, A. P., Menou, K., & Cho, J. Y.-K. 2008, in Astronomical Society of the Pacific Conference Series, Vol. 398, Extreme Solar Systems, ed. D. Fischer, F. A. Rasio, S. E. Thorsett, & A. Wolszczan, 419–+

Showman, A. P. & Polvani, L. M. 2011, *ApJ*, 738, 71

Spiegel, D. S., Silverio, K., & Burrows, A. 2009, *ApJ*, 699, 1487

Stiel, L. & Thodos, G. 1963, Industrial and Engineering Chemistry Fundamentals, 2, 233

Todorov, K., Deming, D., Harrington, J., et al. 2010, *ApJ*, 708, 498

A Appendix: Departure from the Cunningham velocity

The Cunningham velocity is the equivalent of the Stokes velocity for low pressure environnement. Therefore it is not valid for turbulent flow and other expressions may be used when the Reynolds number increases. Here we derive better laws for intermediate and big Reynolds number.

Low Knudsen number

When increasing the reynolds number, the non linear terms of the Navier-Stokes equation becomes more important. We used tabulated values of the drag coefficient in function of the Reynolds number given by Pruppacher & Klett (1978). We assumed that $C_D = 24$ when $N_{R_e} = 1$ to stay coherent with stokes flow and that C_D reaches its asymptotic value $C_D = 0.45$ when $N_{R_e} = 1000$. We obtain :

$$\log_{10}(N_{R_e}) = -1.215047 + 0.923242 \log_{10}(C_D N_{R_e}^2) - 0.031293 \log_{10}(C_D N_{R_e}^2)^2 \tag{30}$$

Then we follow the same method as Ackerman & Marley (2001) noting that :

$$C_D N_{R_e}^2 = \frac{32 \rho g a^3 (\rho_p - \rho)}{3\eta^2} \tag{31}$$

is independent of the velocity, we use the fit of equation 30 and extract the velocity :

$$V_f = \frac{\eta}{2\rho a} 10^{-1.21 + 0.92 \log_{10}(\frac{32\rho g a^3 \Delta\rho}{3\eta^2}) - 0.031 \log_{10}(\frac{32\rho g a^3 \Delta\rho}{3\eta^2})^2} \tag{32}$$

High Knudsen number

In the free-molecular regime, calculations have been made by Probstein (1968) leading to an expression for the drag coefficient :

$$C_D = \frac{2}{3s_a}\sqrt{\pi} + \frac{2s_a^2 + 1}{s_a^3\sqrt{\pi}} \exp(-s_a^2) + \frac{4s_a^4 + 4s_a^2 - 1}{2s_a^4} erf(s_a) \tag{33}$$

where s_a is the ratio of the object velocity over the thermal speed of the gas ($V_T = \sqrt{\frac{2k_B T}{m}} = \frac{\sqrt{\pi}}{2}\bar{c}$) and erf is the error function.

Low velocity limit

When looking at the limit for low velocities, one have to use an equivalent of the error function in 0 :

$$erf(s_a) = \frac{2}{\sqrt{(}\pi)} e^{-s_a^2}(s_a + \frac{2}{3}s_a^3) + o(s_a^4) \tag{34}$$

When using this equations inside equation 33 the term in e^{-s_a} goes to 1 and the terms proportional to $\frac{1}{s_a^3}$ cancels then :

$$C_D \sim \left(\frac{2\sqrt{\pi}}{3} + \frac{16}{3\sqrt{\pi}}\right)\frac{1}{s_a} \tag{35}$$

Using the expression for the thermal speed and noting that for low Knudsen number the viscosity can be approximated by (Chapman & Cowling (1970)) :

$$\eta \approx \frac{1}{2}\rho\lambda\bar{c} \tag{36}$$

we obtain :

$$C_D \sim \left(\frac{2\sqrt{\pi}}{3} + \frac{16}{3\sqrt{\pi}}\right)\frac{\sqrt{\pi}}{2}\frac{2\eta}{\rho V\lambda} \tag{37}$$

which is :

$$C_D \sim \left(\frac{2\sqrt{\pi}}{3} + \frac{16}{3\sqrt{\pi}}\right)2\sqrt{\pi}\frac{1}{N_{R_e}K_N} \tag{38}$$

Then the limit for the drag coefficient at low Knudsen number is :

$$C_D \sim \frac{C_{Dstokes}}{1.61K_N} \tag{39}$$

When comparing this equation with the limit of equation 3 for high Knudsen number there is a remarkable agreement between the two expressions.

High velocity limit

When s_a goes to infinity, the limit of equation 33 is :

$$C_D \sim 2 \tag{40}$$

General case

In order to simplify equation 33 with decided do use the following expression for the drag coefficient at high Knudsen number :

$$C_D = \left(\frac{2\sqrt{\pi}}{3} + \frac{16}{3\sqrt{\pi}}\right)\frac{V_T}{V} + 2 \tag{41}$$

$$C_D = \left(\frac{2\sqrt{\pi}}{3} + \frac{16}{3\sqrt{\pi}}\right)\frac{\sqrt{2k_BT/m}}{V} + 2 \tag{42}$$

Our approximation fits correctly the exact expression in the limit of low and high velocities. In between the difference between the exact expression and our approximation is at most 30%. Replacing C_D by its value in equation 6 we obtain a second order equation for the velocity :

$$2\left(\frac{V}{V_T}\right)^2 + \left(\frac{2\sqrt{\pi}}{3} + \frac{16}{3\sqrt{\pi}}\right)\frac{V}{V_T} - \frac{8}{3}ag\frac{\Delta\rho}{\rho} = 0 \tag{43}$$

which leads to :

$$V_f = \frac{V_T A}{4}\left(\sqrt{1 + \frac{63}{3A^2}ag\frac{\Delta\rho}{\rho V_T^2}} - 1\right) \tag{44}$$

with $A = \left(\frac{2\sqrt{\pi}}{3} + \frac{16}{3\sqrt{\pi}}\right)$.

We can rewrite this equation in term of non-dimensional quantities :

$$V_f = \frac{A}{4}V_T\left(\sqrt{1 + \frac{96}{A^2\sqrt{\pi}}\frac{V_{stokes}}{V_T}K_N} - 1\right) \tag{45}$$

In the limit of small speeds ($V_{stokes} << V_T$) we obtain :

$$V_f = \frac{96}{8\sqrt{\pi}A} K_N V_{stokes} \approx 1.61 K_N V_{stokes} \tag{46}$$

which is in a good agreement with equation 15

In the limit of big speeds ($V_{stokes} >> V_T$) we have a constant drag coefficient $C_D = 2$ so we obtain :

$$V_f = \sqrt{\frac{8ga\Delta\rho}{3C_D\rho}} \tag{47}$$

Velocity plot in the pressure-size plane

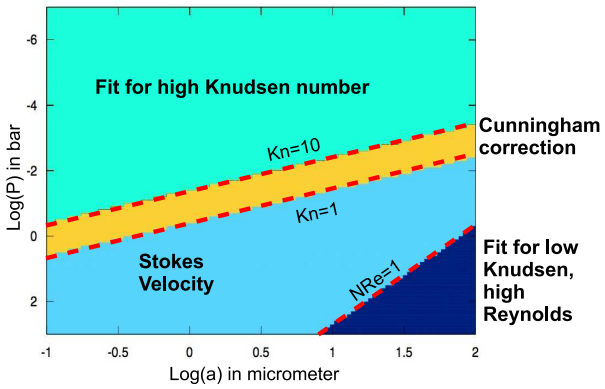

Figure 9: Validity of each solution for the velocity

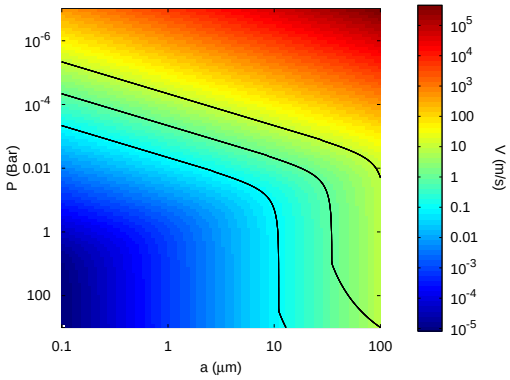

Figure 10: Terminal velocity for particles in different size at different pressure. The plain lines represents contour of 0.1, 1 and 100m/s respectively.

Discussion about the velocity

Figure 11 show the ratio of the cunnhingham velocity to the velocity laws derived before. The difference is noticeable only for particles of the order of $100\mu m$ on top of the 10^{-4} bars level and below the 1 bar lever. This difference is always less than an order of magnitude and concern only a tiny portion of the parameter space. So we decided to neglect it and use only the Cunningham velocity.

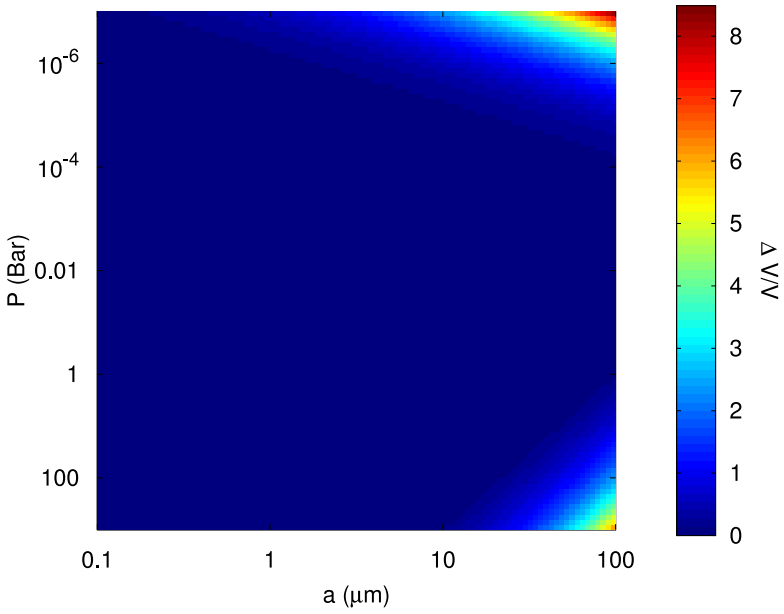

Figure 11: Relative difference between the Cunningham velocity and the more sophisticated models.